Science of the Total Environment 772 (2021) 144957

Contents lists available at ScienceDirect

Science of the Total Environment

journal homepage: www.elsevier.com/locate/scitotenv

Exposure to short-chain chlorinated paraffins inhibited PPARα-mediated fatty acid oxidation and stimulated aerobic glycolysis *in vitro* in human cells

Yufeng Gong [a,b], Ningbo Geng [a], Haijun Zhang [a,*], Yun Luo [a,c], John P. Giesy [b,d], Shuai Sun [a,c], Ping Wu [a], Zhengkun Yu [a], Jiping Chen [a]

[a] CAS Key Laboratory of Separation Sciences for Analytical Chemistry, Dalian Institute of Chemical Physics, Chinese Academy of Sciences, Dalian, Liaoning, China
[b] Toxicology Centre, University of Saskatchewan, Saskatoon, SK, Canada
[c] University of Chinese Academy of Sciences, Beijing, China
[d] Department of Veterinary Biomedical Sciences, University of Saskatchewan, Saskatoon, SK, Canada

HIGHLIGHTS

- Exposure to SCCPs down-regulated expressions of hPPARα target genes.
- Exposure to SCCPs caused a suppressive effect on fatty acid oxidation.
- SCCPs with greater chlorine content had stronger effects on lipid metabolism.
- SCCPs induced a shift in carbohydrate metabolism from TCA cycle to aerobic glycolysis.

GRAPHICAL ABSTRACT

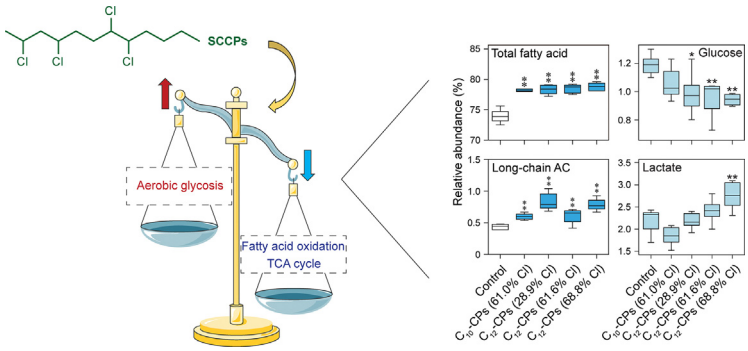

ARTICLE INFO

Article history:
Received 4 November 2020
Received in revised form 29 December 2020
Accepted 30 December 2020
Available online 1 February 2021

Editor: Jay Gan

Keywords:
SCCPs
Human PPARα
Metabolomics
Fatty acid oxidation
Glycolysis

ABSTRACT

Short-chain chlorinated paraffins (SCCPs) could disrupt fatty acid metabolism in male rat liver through activating rat PPARα signaling. However, whether this mode of action can translate to humans remained largely unclear. In this study, based on luciferase assays, $C_{10–13}$-CPs (56.5% Cl) at concentrations greater than 1 μM (i.e., 362 μg/L) showed weak agonistic activity toward human PPARα (hPPARα) signaling. But in HepG2 cells, exposure to $C_{10–13}$-CPs (56.5% Cl) at the human internal exposure level (100 μg/L) down-regulated expressions of most of the tested hPPARα target genes, which encode for enzymes that oxidize fatty acids. In line with the gene expression data, metabolomics further confirmed that exposure to four SCCP standards with varying chlorine contents at 100 μg/L significantly suppressed oxidation of fatty acids in HepG2 cells, mainly evidenced by elevations in both total fatty acids and long-chain acylcarnitines. In addition, exposure to these SCCPs also caused a shift in carbohydrate metabolism from the tricarboxylic acid cycle (TCA cycle) to aerobic glycolysis. Overall, the results revealed that SCCPs could inhibit hPPARα-mediated fatty acid oxidation, and stimulated aerobic glycolysis in HepG2 cells.

1. Introduction

Short-chain chlorinated paraffins (SCCPs) are a group of polychlorinated *n*-alkanes with a length of 10–13 carbon atoms and

* Corresponding author at: CAS Key Laboratory of Separation Sciences for Analytical Chemistry, Dalian Institute of Chemical Physics, Chinese Academy of Sciences, 457 Zhongshan Road, Dalian, China.
E-mail address: hjzhang@dicp.ac.cn (H. Zhang).

https://doi.org/10.1016/j.scitotenv.2021.144957
0048-9697/

general chlorine content of 30%–70% by mass (Fiedler, 2010). SCCPs are widely used in metal-working fluids, flame retardants, and plasticizers (Feo et al., 2009). Previous studies have shown that SCCPs can persist in the environment, bioaccumulate and biomagnify through the food chain, and transport in long range (Du et al., 2020; Li et al., 2016; Zeng et al., 2017). In May 2017, SCCPs were listed as a new group of persistent organic pollutants (POPs) by the Stockholm Convention (UNEP, 2017).

Exposure of humans to SCCPs through diet and ingestion of dust has been demonstrated (Cao et al., 2019; Gao et al., 2018; Sprengel et al., 2019; Zheng et al., 2020b). For example, the mean concentrations of SCCPs in raw cow milk from industrial areas was determined to be 1670 ng/g lipid (Dong et al., 2020), and the estimated daily intake (EDI) of SCCPs through dietary intake for humans was 3109 ng/kg/day (Li et al., 2020). As a result, SCCPs were detected at concentrations of 131–16,100, 370–35,000, and 3750–40,500 ng/g lipid weight in human blood, mother's milk, and cord serum, respectively (Li et al., 2017; Qiao et al., 2018; Xia et al., 2017). Ubiquitous exposure to SCCPs has raised concerns about risks to human health. However, knowledge of the potentially toxic effects of internal SCCPs exposure on humans has remained quite limited.

SCCPs have been found to have developmental and reproductive toxicity, immune-toxicity, endocrine-disrupting activity, carcinogenicity, and biological properties to disrupt cellular metabolism (Ali and Legler, 2010; Gong et al., 2018; Liu et al., 2016; Wang et al., 2018; Zhang et al., 2016). Peroxisome proliferator-activated receptors (PPARs) belonging to the nuclear receptor superfamily are ligand-activated transcription factors, and they include three subtypes, i.e., α, δ/β, and γ (Kersten, 2014). It has been revealed that PPARs play a crucial role in lipid metabolism and energy homeostasis (Poulsen et al., 2012). Besides, PPARs are also involved in pathogenesis of several chronic human diseases such as diabetes, obesity, atherosclerosis and cancer (Kersten et al., 2000). By using molecular docking analysis, our previous study revealed that SCCPs have strong binding affinities to PPARα via hydrophobic contacts while no hydrogen-bond interactions were found between SCCPs and the ligand-dependent activation function (AF-2) region (Gong et al., 2019). Through this unconventional binding mode, SCCPs could accelerate fatty acid oxidation in rat liver by activating rat PPARα-mediated pathway (Geng et al., 2019). However, rodents are thought to be more responsive to PPAR activators than are primates (Klaunig et al., 2003), which raises the question of whether this mode of action might translate to humans. For example, exposure to diethylhexyl phthalate (DEHP) protected mice against diet-induced obesity through PPARα-dependent activation of fatty acid catabolism in the liver, which didn't extend to humans (Feige et al., 2010). Transactivation activity of SCCPs to human PPARα (hPPARα) is still unknown. Whether activation of hPPARα is associated with SCCPs-induced toxicity in humans needs to be clarified.

As an attempt to solve this issue, the activation potency of SCCPs against hPPARα was first determined by the luciferase reporter gene assay in this study. Then, the effects of SCCPs exposure on expressions of PPARα target genes in HepG2 cells were measured to verify the potential hPPARα activation activity of SCCPs. Finally, the effects of four SCCPs standards with varying chlorine contents on metabolism of HepG2 cells were characterized and compared by a pseudo-targeted metabolomics approach. The obtained data provided a better understanding of the toxicity of SCCPs in humans and could be helpful for the human health risk assessment of SCCPs.

2. Materials and methods

2.1. Chemicals

Five kinds of SCCP mixture standards, i.e., C_{10-13}-CPs (C_{10}-CPs:C_{11}-CPs:C_{12}-CPs:C_{13}-CPs mass ratio = 1:1:1:1; Cl content: 56.5%), C_{10}-CPs (Cl content: 61.0%), C_{12}-CPs (Cl content: 28.9%), C_{12}-CPs (Cl content: 61.6%), and C_{12}-CPs (Cl content: 68.8%), were synthesized by chlorination of *n*-alkane according to a previously published method (Tomy et al., 2000). Hendecanoic acid, nonadecanoic acid, L-phenylalanine-D^5, (8,8,8-D^3)-L-carnitine, 1,2-Diheptadecanoyl-sn-glycero-3-phosphoethanolamine, and 1-lauroyl-2-hydroxy-sn-glycero-3-phosphocholine, purchased from Sigma (Shanghai, China), were used as internal standards for metabolome profiling. Methanol, water, and acetonitrile were of LC-MS grade from Fisher Scientific (Schwerte, Germany).

2.2. Cell culture conditions

Human embryonic kidney 293 T cells and HepG2 cells were obtained from China Infrastructure of Cell Line Resources (Shanghai, China). Dulbecco Modified Eagle Medium (DMEM; Gibco-BRL, USA) supplemented with 10% fetal bovine serum and 1% penicillin-streptomycin (Beyotime, China) was employed for cell culture. All cells were cultured under a humidified environment of 5% CO_2 at 37 °C.

2.3. Luciferase assay

Human derived peroxisome proliferator response element (PPRE)-firefly luciferase reporter plasmids (pGL4.26-/hPPRE-Luc) and human PPARα ligand-binding domain (LBD) expression plasmid (p3xFlag-rPPARα/hPPARα) were obtained from TranSheep company (Shanghai, China). 293 T cells (1×10^4/well in 24-well plates) were transiently co-transfected with 90 ng of luciferase reporter plasmid and 5 ng of expression plasmid, either empty or coding for hPPARα LBD using Lipofectamine 2000 reagent (Life Technologies). Afterward, the culture medium was replaced, and the cells were treated with test chemicals for 24 h to determine the potential PPARα agonistic activities. Dimethyl sulfoxide (DMSO) and pirinixic acid served as negative and positive control, respectively. All transfections and treatments were conducted in triplicate. After exposure, luciferase activities were measured by a luciferase reporter assay kit (Promega, USA). The luciferase activity in negative control group was assigned as one.

2.4. SCCPs exposure experiment

HepG2 cells at exponential growth phase were plated in 6-well plates at a density of 4×10^5/well and allowed to reach 80% confluency. Then, cells were treated with C_{10-13}-CPs (Cl content: 56.5%) for gene expression analysis; or treated with C_{10}-CPs (Cl content: 61.0%), C_{12}-CPs (Cl content: 28.9%), C_{12}-CPs (Cl content: 61.6%), or C_{12}-CPs (Cl content: 68.8%) for metabolomics analysis. DMSO (0.1%) was used as vehicle control. The exposure concentration of all SCCPs treatments was 100 μg/L, which was comparable to the median value of detected ∑SCCPs in human blood (range: 14–3500 ng/g; median value: 98 ng/g) (Li et al., 2017). After 24 h exposure, cells were washed three times in cold phosphate-buffered saline (PBS) for gene expression analysis; or in cold ultrapure water for metabolomic analysis. All samples were stored at −80 °C until further treatment.

2.5. Quantitative real-time polymerase chain reaction (qPCR) analysis

Total RNA was isolated by use of Takara RNAiso plus reagent (Takara, Tokyo, Japan). RNA quality and concentration were determined by spectrophotometric analysis (Agilent 2100 Bioanalyzer, Agilent Technologies, Palo Alto, CA) and 1% agarose gel electrophoresis. qPCR was performed on the Light Cycler 480 PCR System (Roche Diagnostics, Mannheim, Germany) with a FastStart Universal SYBR GreenMaster kit (Roche Applied Science, Mannheim, Germany). Housekeeping glyceraldehyde-3-phosphate dehydrogenase (*GAPDH*) was used as the reference gene. All gene mRNA levels were normalized by the $2^{-\Delta\Delta Ct}$ method (Livak and Schmittgen, 2001). The primers used are listed in Table S1 of Supplementary materials.

2.6. Pseudo-targeted metabolomics analysis

Metabolites were first extracted with a mixture of methanol/water (4:1, v:v), and then applied to a pseudo-targeted metabolomics workflow (Zheng et al., 2020a). Details on the preparation of samples and instrumental analysis are given in Supplementary materials. Metabolite annotation was done by MS/MS matching to experimental spectra in the Human Metabolome Database (HMDB). Commercially available standards were used to further validate these annotations during the method development stage (Wang et al., 2016). Raw metabolomics data was processed by use of MultiQuant software (3.0.1, AB SCIEX). After peak alignment and missing value interpolation, peak areas of each metabolite were normalized to corresponding internal standards and then normalized to the sum of each sample. Besides, quality controls (QC) samples were prepared by pooling 20 μL of aliquots from each sample. QC samples were analyzed before analysis of actual biological samples for system equilibration and inserted after every six samples to monitor system stability during run. Procedural blank samples (i.e., extraction without actual sample) were also prepared and analyzed to filter any contaminations that were introduced during sample preparation.

2.7. Statistics

All data are presented as mean ± standard deviation (SD). Differences were considered significant at $0.01 < P < 0.05$ and highly significant when $P < 0.01$. For metabolomics data, data were log-transformed to achieve normally distributed data before statistical analysis. Partial least squares discriminate analysis (PLS-DA) was generated after autoscaling of the metabolomics data by the online MetaboAnalyst platform (Chong et al., 2018). The metabolic effect level index (MELI) proposed by Riedl et al. (2015) was also calculated for each exposure group. After testing for the normality distribution (Kolmogorov-Smirnov test) and variance homogeneity (Levene test), one-way ANOVA followed by Student's *t*-test were conducted to evaluate the significance of the mean differences. Differential metabolites (DMs) were determined with the criteria of false discovery rate (FDR) < 0.05 and a variable importance in the project (VIP) value of >0.75. DMs were further applied to KEGG pathway enrichment analysis, and a *P* value <0.05 was adopted as the threshold for significant enrichment. In addition, chemical similarity enrichment analysis (ChemRICH), which enables study-specific and background-independent enrichment analysis, was also performed on the annotated metabolomics dataset (Barupal and Fiehn, 2017). Chemical clusters with FDR < 0.05 and cluster size >4 were considered significant. Cluster direction is determined by the median $\log_2$ fold change relative to control of DMs in each metabolite cluster (Contrepois et al., 2020). Pearson correlation analysis and related *P* value were used to describe the correlations.

3. Results and discussion

3.1. Activity of SCCPs toward hPPARα transactivation

The ability of SCCPs to modulate hPPARα activity was first determined by an hPPARα-mediated luciferase reporter gene assay. $C_{10–13}$-CPs (56.5%Cl) was employed as the test chemical to represent a real scenario exposure to SCCPs mixtures in humans. The concentrations of SCCPs were set at 0.1 μM (36 μg/L), 1 μM (362 μg/L), 2 μM (723 μg/L) and 5 μM (1808 μg/L), respectively. Before the luciferase assays, effects of exposure on cell viability were evaluated by use of MTT assays. No significant cytotoxicity was observed in 293 T cells exposed to $C_{10–13}$-CPs (56.5% Cl) at 0.01–50 μM for 24 h (Fig. S1). During the luciferase reporter assay, treatment with 1 μM of pirinixic acid, a well-known specific agonist for PPARα, significantly enhanced the hPPARα-mediated luciferase activity, while no significant responses were observed in non-hPPARα transfected cells, indicating the validity of our luciferase assay (Fig. S3).

As shown in Fig. 1, treatment with $C_{10–13}$-CPs (56.5% Cl) at concentrations of ≥1 μM (362 μg/L) induced a weak partial agonistic activity toward hPPARα, with a maximal induction of 1.73 ± 0.02 fold compared to the control. Additionally, compared with the hPPARα transfected cells, luciferase activities in non-hPPARα transfected cells after exposure to SCCPs were significantly lower, implying that the induction of luciferase activity was specific to hPPARα.

3.2. Effects of SCCPs exposure on the expressions of PPARα target genes

To further validate the effects of SCCPs exposure on hPPARα, the expression levels of classical downstream genes of hPPARα signaling were quantified in HepG2 cells after exposure to $C_{10–13}$-CPs mixture (56.5% Cl). Before exposure, cell viability was determined to obtain the optimal exposure concentrations for gene expression analysis. No apparent effects on cell viability were found at SCCPs concentrations less than 100 μg/L (Fig. S2). The exposure concentration of 100 μg/L, which is comparable to the median ∑SCCPs concentration detected in human blood (Li et al., 2017; Ding et al., 2020), was finally selected for the test. The tested genes included *CPT1A* (encoding carnitine palmitoyltransferase 1A), *CPT2* (encoding carnitine palmitoyltransferase 2), *ACSL1* (encoding acyl-CoA synthetase long chain family member 1), *ACOX1* (encoding acyl-CoA oxidase 1), *ACADM* (encoding acyl-CoA dehydrogenase medium chain), *EHHADH* (encoding enoyl-CoA hydratase and 3-hydroxyacyl CoA dehydrogenase), *ACAA1* (encoding acetyl-CoA acyltransferase 1), *ECI1* (encoding enoyl-CoA delta isomerase 1), *APOA5* (encoding apolipoprotein A5), *PLIN2* (emcoding perilipin 2), *GOT1* (encoding glutamic-oxaloacetic transaminase 1), and *ELOVL6* (encoding fatty acid elongase 6). All of these genes were considered to be regulated by PPARα (Kersten, 2014; Mandard et al., 2004; Rakhshandehroo et al., 2010).

Exposure to $C_{10–13}$-CPs (56.5% Cl) at the human internal exposure level (100 μg/L) significantly down-regulated expressions of most of the tested hPPARα target genes in HepG2 cells, including *CPT2*, *ACSL1*, *ACOX1*, *ACADM*, *EHHADH*, and *PLIN2* (Fig. 2). These down-regulated genes are mainly responsible for fatty acid oxidation. Moreover, only mRNA levels of *APOA5* and *ACAA1* were found significantly up-regulated. No changes in mRNA levels of *CPT1A*, *GOT1*, and *ELOVL6* were observed. The altered gene expression profile after exposure to $C_{10–13}$-CPs (56.5% Cl) suggested a suppressive effect of SCCPs on hPPARα signaling in HepG2 cells.

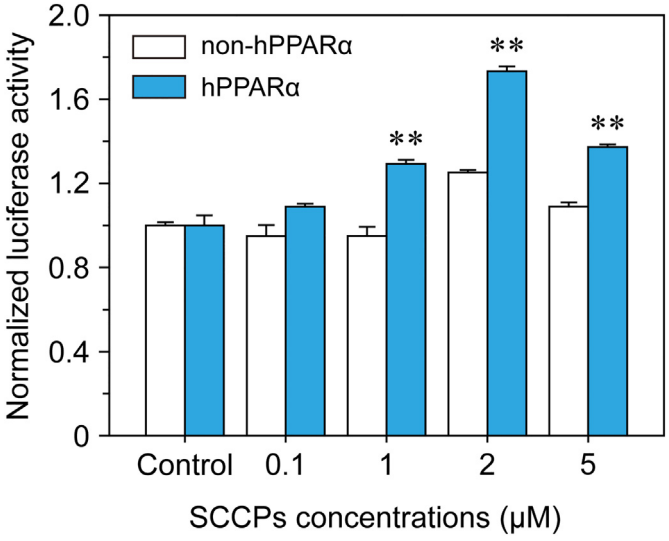

Fig. 1. Effects of $C_{10–13}$-CPs (56.5%Cl) on hPPARα-mediated luciferase transcription activity. The firefly luciferase activity was normalized to the control group (0.1% DMSO). Asterisks indicate statistically significant differences from the control group in hPPARα transfected cells (** $P < 0.01$). $N = 3$.

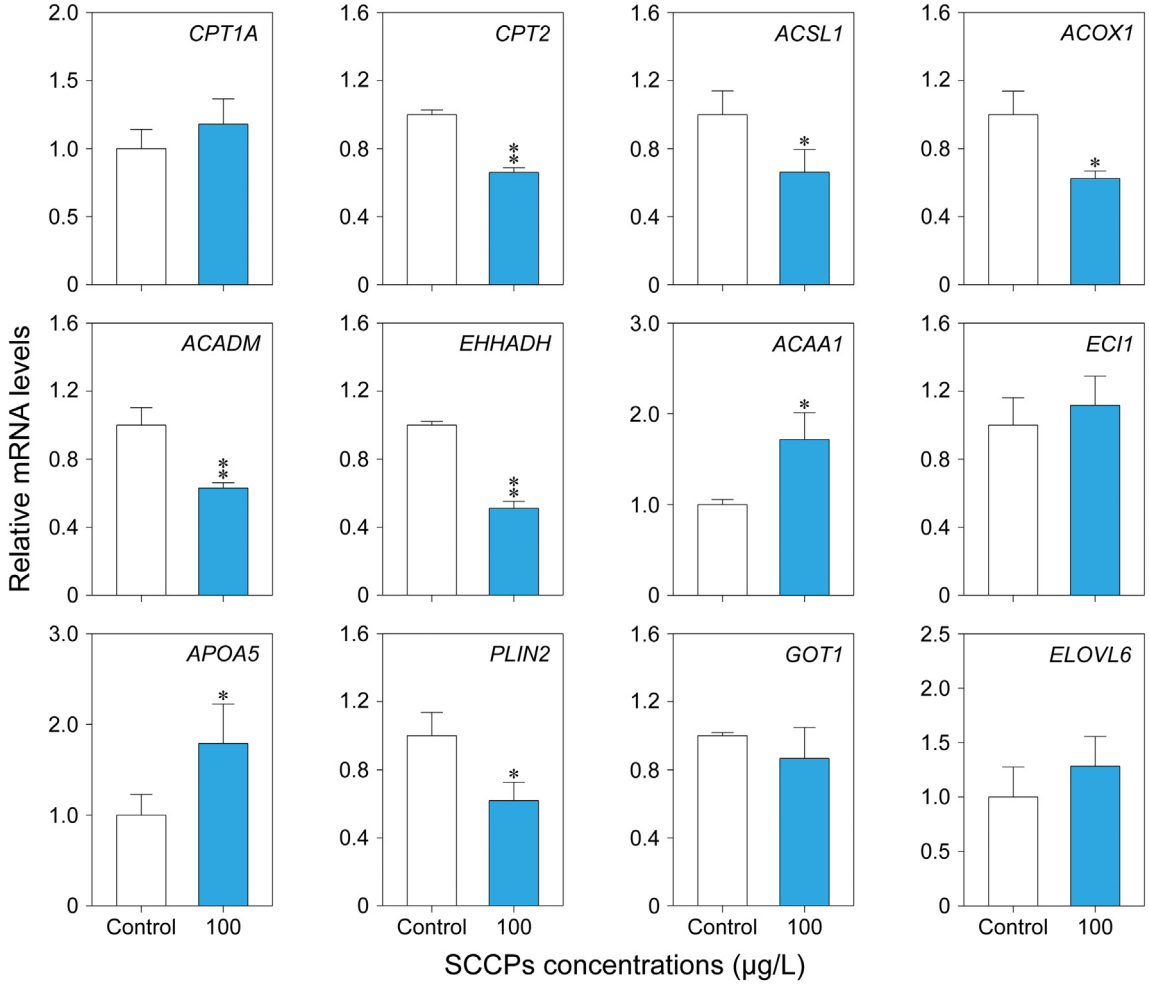

Fig. 2. Quantitative analysis of expressions of classical hPPARα target genes in HepG2 cells treated with 100 μg/L of C_{10-13}-CPs (Cl content: 56.5%) for 24 h. Asterisks indicate statistically significant differences from the control group (*$0.01 < P < 0.05$, **$P < 0.01$). $N = 6$. *CPT1A*: carnitine palmitoyltransferase 1A; *CPT2*: carnitine palmitoyltransferase 2; *ACSL1*: acyl-CoA synthetase long chain family member 1; *ACOX1*: acyl-CoA oxidase 1; *ACADM*: acyl-CoA dehydrogenase medium chain; *EHHADH*: enoyl-CoA hydratase and 3-hydroxyacyl CoA dehydrogenase; *ACAA1*: acetyl-CoA acyltransferase 1; *ECI1*: enoyl-CoA delta isomerase 1; *APOA5*: apolipoprotein A5; *PLIN2*: perilipin 2; *GOT1*: glutamic-oxaloacetic transaminase 1; *ELOVL6*: fatty acid elongase 6.

According to our previous work, SCCPs exhibited remarkable binding affinities to hPPARα protein only via hydrophobic contacts, and no hydrogen bonds were found (Gong et al., 2019). Previous literatures have shown that hydrogen bond interactions with residues on the ligand-dependent activation function (AF-2) region of PPARs are crucial in the initiation of PPAR pathway (Bernardes et al., 2013; Wu et al., 2017). Thus, although SCCPs have strong binding affinities to hPPARα, SCCPs might have only partial activation efficacy at the hPPARα receptor due to the lack of hydrogen bond interactions and less sensitive responsiveness of hPPARα to agonists (Bility et al., 2004; Mukherjee et al., 1994). It is plausible to deduce that SCCPs at low exposure concentrations (e.g., less than 100 μg/L) actually act as competitive antagonists, competing with natural ligands of hPPARα for receptor occupancy and finally lead to suppressive effects on hPPARα signaling cascade. Nevertheless, at high exposure concentrations (e.g., greater than 362 μg/L), SCCPs could induce an extremely weak activation of hPPARα signaling, as observed in our luciferase reporter gene assay (Fig. 1).

3.3. Overall metabolic disorders induced by exposure to SCCPs

Then, we further explored the downstream effects of exposure to SCCPs on lipid metabolism and energy homeostasis in HepG2 cells due to the key roles of hPPARα in these pathways. Four SCCP standards with varying chlorine contents were characterized and compared in this study by a pseudo-targeted metabolomics approach. HepG2 cells were exposed to C_{10}-CPs (61.0% Cl), C_{12}-CPs (28.9% Cl), C_{12}-CPs (61.6% Cl), or C_{12}-CPs (68.8% Cl) at the concentration of 100 μg/L for 24 h. We adopted HepG2 cells to investigate the metabolic disorders induced by SCCPs because liver is the main target organ of SCCPs (UNEP, 2017), and HepG2 cells preserve most hepatic functions and represent an established human liver cell model in toxicological studies (Xia et al., 2016; Yu et al., 2013). QC analysis revealed good repeatability of our metabolomics experiment (Fig. S4). In the present study, 280 metabolites were accurately quantified. The PLS-DA model showed satisfactory explanation, fitness, and prediction power. A clear separation between cells exposed to SCCPs and the control group along component 1 was observed (Fig. 3a), which indicated that exposure of HepG2 cells to SCCPs caused perturbations of intracellular metabolites.

A total of 165 intracellular metabolites were determined to be differential after exposure, which met the criteria of FDR < 0.05 and VIP > 0.75. To further investigate metabolic interference caused by exposure to SCCPs, annotated metabolites were further subjected to ChemRICH analysis, which is based on chemical similarity and ontology mapping. The most significant and largest metabolite sets identified by ChemRICH analysis were quite similar among different treatment groups, indicating a similar metabolomics response of HepG2 cells to SCCPs with varying chlorine contents (Fig. 3b). These significantly altered metabolite sets mainly included phospholipids, fatty acids, and dicarboxylic acids. Moreover,

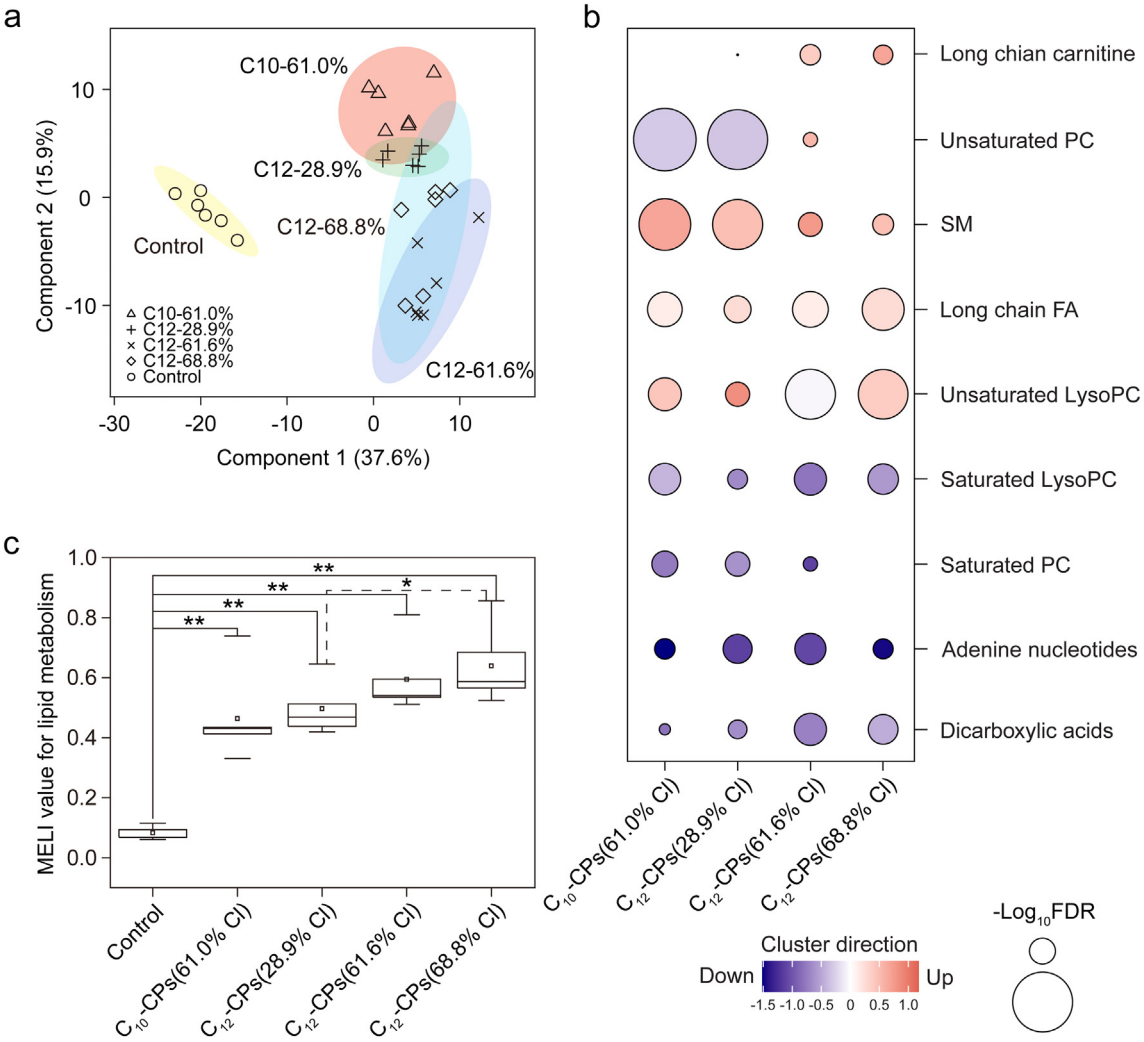

Fig. 3. Changes in metabolome of HepG2 cells after exposure to four SCCP groups with varying chlorine contents. (a) PLS-DA score plot. All data were log-transformed and auto-scaled prior to PLS-DA analysis. $R^2 = 0.93$; $Q^2 = 0.91$. (b) Significantly enriched metabolite clusters by ChemRICH analysis. Pathway direction is the median $\log_2$ fold change of DMs relative to control in each cluster (blue, downregulated; red, up-regulated). Metabolites clusters with FDR < 0.05 and cluster size >4 were treated as significant. The dot size represents significance. (c) MELI values of lipid metabolites in each treatment group. *$0.01 < P < 0.05$; **$P < 0.01$. (For interpretation of the references to colour in this figure legend, the reader is referred to the web version of this article.)

KEGG pathway analysis of identified DMs were also performed. The most relevant pathways disrupted by SCCPs were linoleic acid metabolism; glycine serine and threonine metabolism; nicotinate and nicotinamide metabolism; glycerophospholipid metabolism; alanine, aspartate and glutamate metabolism; and citrate cycle (Fig. S5).

PPARα is the master regulator of lipid metabolism in hepatocytes (Kersten, 2014). Thus, we used the $MELI_{lipid}$ value to assess the overall disruption of lipids by SCCPs. The MELI value converts the information-rich metabolomics data into an integrated and quantitative endpoint, which has been successfully applied in toxicological evaluation (Ren et al., 2018; Wang et al., 2018). Compared to the control, the $MELI_{lipid}$ values in each exposure group were significantly greater (Fig. 3c). Pearson correlation analysis indicated that $MELI_{lipid}$ values were linearly correlated with chlorine contents within C_{12}-CPs groups ($R^2 = 0.94$; $P = 0.03$). This result agreed well with those of previous studies in that binding affinity of SCCPs to hPPARα is dependent on chlorine content (Gong et al., 2019) and further suggested the involvement of hPPARα in SCCPs induced disruption of lipid metabolism in HepG2 cells.

3.4. Effects of SCCPs exposure on fatty acid metabolism

In this study, exposure to SCCPs caused significant increases in contents of intra-cellular total fatty acid (FA) and long-chain fatty acid (LC-FA), but decreased the contents of medium-chain fatty acid (MC-FA) and very long-chain fatty acid (VLC-FA) in HepG2 cells (Fig. 4). Moreover, analysis of acylcarnitine profiles revealed significant increases in long-chain (LC-AC) and medium-chain (MC-AC) species in cells exposed to SCCPs. On the contrary, concentrations of short-chain acylcarnitine (SC-AC) and free L-carnitine in cells exposed to SCCPs were significantly less, relative to those of the control group.

Before being oxidized, LC-FAs must be activated and transported into mitochondrial matrix through the carnitine shuttle system (Wakil and Abu-Elheiga, 2009). In this process, LC-ACs are produced by transesterification of long-chain acyl-CoA, which is regulated by *CPT1A*. Once inside mitochondria, LC-ACs are reconverted into free carnitine and long-chain acyl-CoA by *CTP2*. When fatty acid cannot be broke down efficiently, LC-ACs accumulate in cells whereas amounts of short species and free L-carnitine decrease (Makowski et al., 2009; van VLIES et al., 2005). Thus, the marked elevations in concentrations of total FA and LC-AC observed in this study suggested a suppressive effect of SCCPs on mitochondrial fatty acid oxidation in HepG2 cells. Similarly, treatment with acetaminophen caused irreversible inhibition of fatty acid oxidation in wild type mice, characterized by accumulation of LC-AC and free fatty acids in serum (Chen et al., 2009). It is worth noting that in line with the metabolomics data, several genes that regulate the carnitine shuttle system (i.e., *CPT2*) and fatty acid oxidation

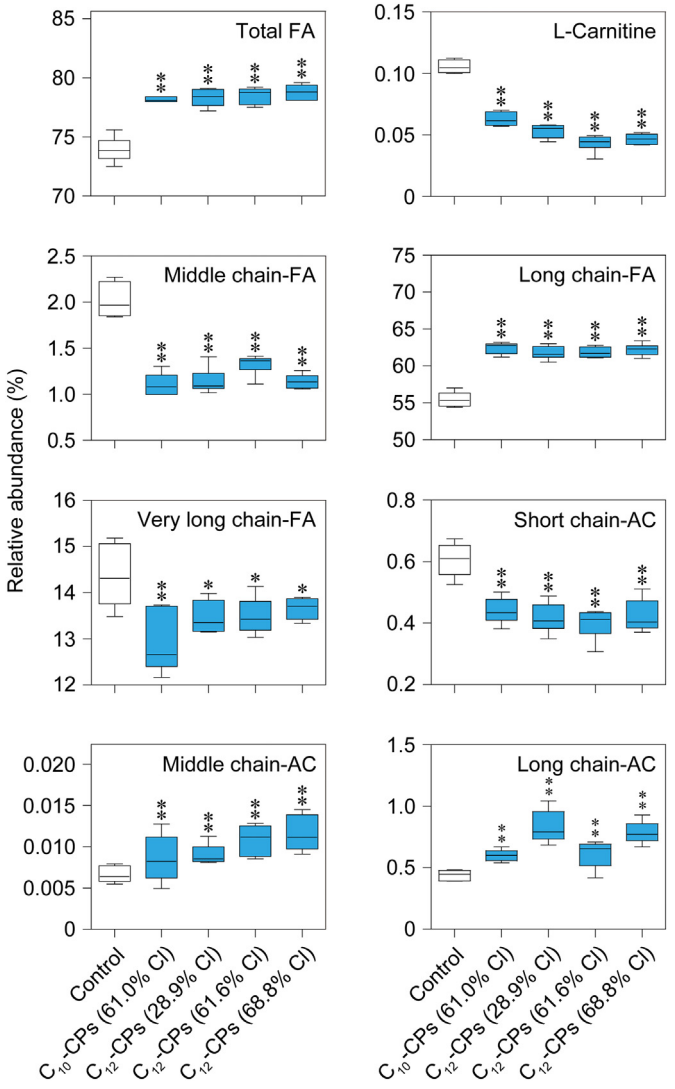

Fig. 4. Effects of exposure to four SCCP groups with varying chlorine contents on metabolism of fatty acids in HepG2 cells. FA: fatty acid; AC: acylcarnitine. Significant differences were indicated in comparison with the control by the *t*-test. * $P < 0.05$; ** $P < 0.01$. $N = 6$.

enzymes (i.e., *ACSL1*, *ACOX1*, *ACADM*, and *EHHADH*) were also significantly down-regulated in HepG2 cells after exposure to 100 μg/L of $C_{10–13}$-CPs (56.5% Cl) (Fig. 2). There is ample evidence that these genes are tightly regulated by hPPARα in liver (Currie et al., 2013; Kersten, 2014; Nguyen et al., 2008). Thus, we speculated that interactions between SCCPs and hPPARα might be responsible for the impaired fatty acids oxidation in HepG2 cells.

3.5. Effects of SCCPs on glycolysis and tricarboxylic acid cycle (TCA cycle)

In recent years, emerging evidence has shown that several crucial genes involved in metabolism of glucose are regulated by PPARα in a direct or indirect way, which suggests a role of PPARα in modulating glucose homeostasis (Hong et al., 2019; Peeters and Baes, 2010). For example, activation of PPARα by exposure to PPARα agonists could reduce expression of pyruvate kinase and down-regulate glycolysis in primary hepatocytes or rats (Gustafson et al., 2002; Pan et al., 2000; Xu et al., 2006). In addition, results of previous studies also suggest that hepatic gluconeogenesis is directly targeted by PPARα (Rakhshandehroo et al., 2007). In this study, disorders of glucose metabolism were also observed in HepG2 cells after exposure to SCCPs (Fig. 5). Exposure to all three C_{12}-CP standards significantly decreased intracellular concentrations of glucose in HepG2 cells, while no significant change was observed after exposure to C_{10}-CPs (61.0% Cl). Moreover, compared to the controls, only C_{12}-CPs (68.8% Cl) having the greatest chlorine content caused a significant increase in concentrations of lactate. These results indicated that SCCPs with greater carbon chain length and chlorine content have stronger effects on glycolysis. Our findings depicted the decreased glucose level with a subsequent elevation in lactate in cells exposed to C_{12}-CPs (68.8% Cl), which suggested up-regulation in glycolysis in HepG2 cells. Concurrently, several metabolites involved in the glycolysis pathway, namely glucose 6-phosphate, fructose 6-phosphate, glyceraldehyde 3-phosphate, and glycerate 3-phosphate, were also significantly altered by treatments with C_{12}-CPs, which further confirmed disturbance of glycolysis.

In addtion, data on metabolomics revealed a down-regulation in TCA cycle pathway upon SCCPs exposure. Notebly, constitutes of the TCA cycle, including citrate, cis-aconitate, isocitrate, oxoglutaric acid, fumarate, and malate were all significantly decreased in SCCPs exposure groups in relative to the control. Citrate is an important intermediate in the TCA cycle which mainly derives from oxaloacetate and its precursor pyruvate. The lesser concentration of citrate in cells exposed to C_{12}-CPs (68.8% Cl) might be a result of lesser accessbility of pyruvate due to enhanced formation of lactate in HepG2 cells after exposure. These results suggested an enhanced shift in energy production from the TCA cycle to aerobic glycolysis. In general, the TCA cycle is the hub of energy output in cellular metabolism. However, most tumor cells produce energy mainly through glycolysis during which glucose is converted into lactate in cytoplasm even under aerobic conditions (Gatenby and Gillies, 2004). This specific feature of metabolism, also known as "Warburg effect", could contribute to rapid proliferation of tumor cells (Lunt and Vander Heiden, 2011). The findings of the study could provide new insights into carcinogenic effects of SCCPs (Bucher et al., 1987; Serrone et al., 1987).

4. Implications for health of humans

With wide use of SCCPs in industrial applications, concentrations of SCCPs have been reported in air (Li et al., 2012), sea water (Ma et al., 2014), soil (Xu et al., 2016), indoor dust, diet, drinking water (Gao et al., 2018) and in wildlife (Li et al., 2019). In human blood, milk, and cord serum, the ∑SCCPs concentrations could reach to 131–16,100, 370–35,000, and 3750–40,500 ng/g lipid weight, respectively (Li et al., 2017; Qiao et al., 2018; Xia et al., 2017). It is noteworthy that concentrations of SCCPs in human tissues are comparable to the exposure dose used in the present study and thereby might already be sufficient to disrupt the normal cellular metabolism in humans. PPARα plays a crucial role in transcriptional regulation of lipid and energy homeostasis in liver (Kersten, 2014). PPARα also improves atherosclerosis and insulin resistance, and provides anti-inflammatory effects (Kersten et al., 2000; Zandbergen and Plutzky, 2007). Dysfunctions in PPARα activity caused by exposure to environmental chemicals have been implicated in the development of human diseases (Lau et al., 2010). For example, monoethylhexyl phthalate (MEHP) could act through activating the PPARα and PPARγ signaling pathway to suppress aromatase transcription and estradiol production, finally leading to anovulation (Lovekamp-Swan and Davis, 2003). In the present study, we are the first to report that SCCPs have extremely weak activation potency toward hPPARα and exposure to SCCPs at the human internal exposure level could inhibit fatty acid oxidation in HepG2 cells probably by interacting with hPPARα signaling. In addition, exposure to these SCCPs also caused a shift in carbohydrate metabolism from TCA cycle to aerobic glycolysis. Our findings imply important environmental risks of SCCPs to human health. One possible limitation of our study is that the expression of hPPARα gene in *in vitro* cultured human hepatocytes is much lower as compared to that in human liver (Kersten and Stienstra, 2017). In the future, more efforts should

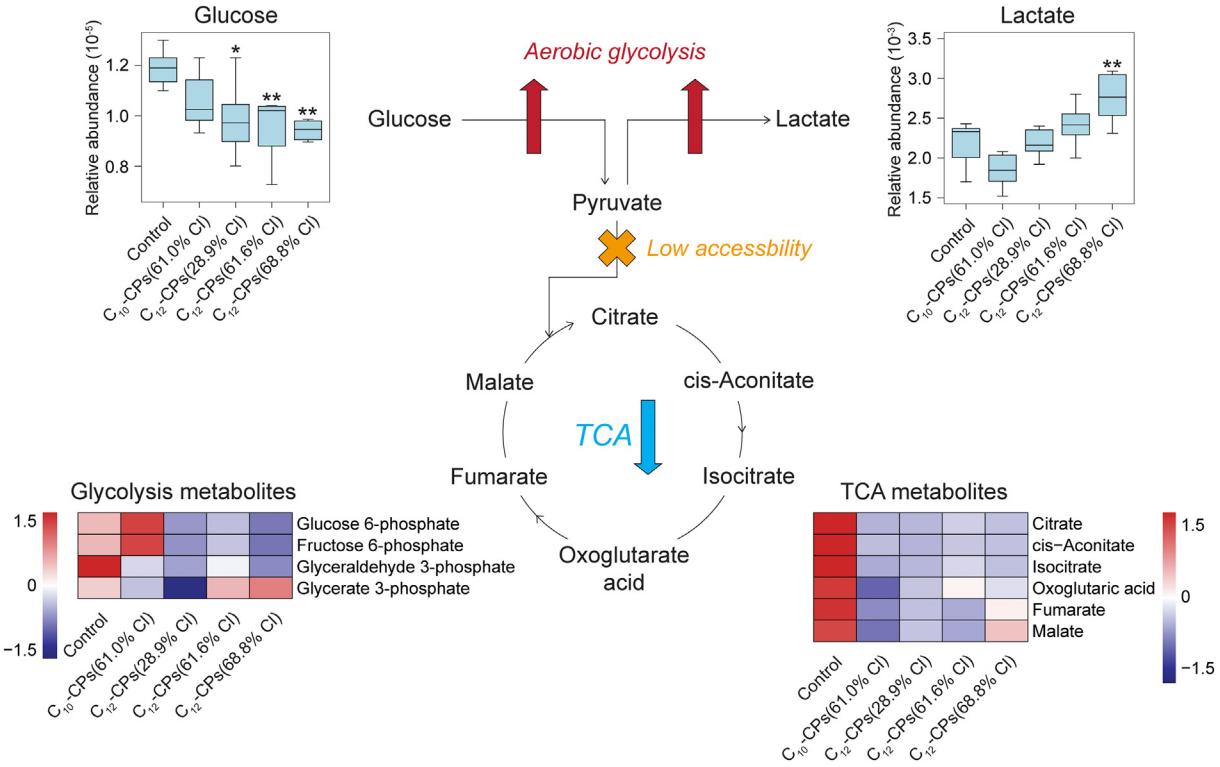

Fig. 5. Metabolic disorders of glycolysis and TCA cycle after exposure to four SCCP groups with varying chlorine contents. Significant differences versus control are indicated by Student's *t*-test. * $P < 0.05$; ** $P < 0.01$. $N = 6$. Data were log-transformed and auto-scaled in prior to heatmap analysis.

be paid to further investigate the adverse effects of SCCPs exposure on metabolism homeostasis in humans by using multi-omics techniques.

Funding

This work was financially supported by the National Natural Science Foundation of China (grant nos. 21707140, 21337002, and 21277141), and the Chinese National Basic Research Program (grant nos. 2015CB453100). Prof. John P. Giesy was supported by the Canada Research Chairs Program of the Natural Science and Engineering Research Council of Canada.

Declaration of competing interest

The authors declare that they have no known competing financial interests or personal relationships that could have appeared to influence the work reported in this paper.

Appendix A. Supplementary data

Primer sequences for qPCR; Sample preparation and instrumental analysis for metabolomics analysis; Calculation for metabolic effect level index (MELI); MTT assays; Validity of luciferase assay; Repeatability of pseudo-targeted metabolomics; KEGG pathway analysis of differential metabolites (DMs). Supplementary data to this article can be found online at doi: https://doi.org/10.1016/j.scitotenv.2021.144957.

References

Ali, T.E.S., Legler, J., 2010. Overview of the mammalian and environmental toxicity of chlorinated paraffins. In: Boer, J. (Ed.), Chlorinated Paraffins. Springer, Berlin Heidelberg, Berlin, Heidelberg, pp. 135–154.

Barupal, D.K., Fiehn, O., 2017. Chemical similarity enrichment analysis (ChemRICH) as alternative to biochemical pathway mapping for metabolomic datasets. Sci. Rep. 7, 14567.

Bernardes, A., Souza, P.C.T., Muniz, J.R.C., Ricci, C.G., Ayers, S.D., Parekh, N.M., Godoy, A.S., Trivella, D.B.B., Reinach, P., Webb, P., Skaf, M.S., Polikarpov, I., 2013. Molecular mechanism of peroxisome proliferator-activated receptor α activation by WY14643: a new mode of ligand recognition and receptor stabilization. J. Mol. Biol. 425, 2878–2893.

Bility, M.T., Thompson, J.T., McKee, R.H., David, R.M., Butala, J.H., VandenHeuvel, J.P., Peters, J.M., 2004. Activation of mouse and human peroxisome proliferator-activated receptors (PPARs) by phthalate monoesters. Toxicol. Sci. 82, 170–182.

Bucher, J.R., Alison, R.H., Montgomery, C.A., Huff, J., Haseman, J.K., Farnell, D., Thompson, R., Prejean, J.D., 1987. Comparative toxicity and carcinogenicity of two vhlorinated paraffins in F344/N rats and B6C3F1 mice. Toxicol. Sci. 9, 454–468.

Cao, D., Gao, W., Wu, J., Lv, K., Xin, S., Wang, Y., Jiang, G.B., 2019. Occurrence and human exposure assessment of short- and medium-chain chlorinated paraffins in dusts from plastic sports courts and synthetic turf in Beijing. China. Environ. Sci. Technol. 53, 443–451.

Chen, C., Krausz, K.W., Shah, Y.M., Idle, J.R., Gonzalez, F.J., 2009. Serum metabolomics reveals irreversible inhibition of fatty acid β-oxidation through the suppression of PPARα activation as a contributing mechanism of acetaminophen-induced hepatotoxicity. Chem. Res. Toxicol. 22, 699–707.

Chong, J., Soufan, O., Li, C., Caraus, I., Li, S., Bourque, G., Wishart, D.S., Xia, J.G., 2018. MetaboAnalyst 4.0: towards more transparent and integrative metabolomics analysis. Nucleic Acids Res. 46, W486–W494.

Contrepois, K., Wu, S., Moneghetti, K.J., Hornburg, D., Ahadi, S., Tsai, M.-S., et al., 2020. Molecular choreography of acute exercise. Cell 181, 1112–1130.

Currie, E., Schulze, A., Zechner, R., Walther, T.C., Farese, R.V., 2013. Cellular fatty acid metabolism and cancer. Cell Metabo. 18, 153–161.

Ding, L., Luo, N., Liu, Y., Fang, X., Zhang, S., Li, S., Jiang, W., Zhao, N., 2020. Short and medium-chain chlorinated paraffins in serum from residents aged from 50 to 84 in Jinan, China: occurrence, composition and association with hematologic parameters. Sci. Total Environ. 728, 137998.

Dong, S., Zhang, S., Li, X., Wei, S., Li, T., Zou, Y., Zhang, W., Cheng, J., Wang, R., Wang, P., Su, X., 2020. Occurrence of short- and medium-chain chlorinated paraffins in raw dairy cow milk from five Chinese provinces. Environ. Int. 136, 105466.

Du, X., Yuan, B., Zhou, Y., de Wit, C.A., Zheng, Z., Yin, G., 2020. Chlorinated paraffins in two snake species from the Yangtze River delta: tissue distribution and biomagnification. Enviro. Sci. Technol. 54, 2753–2762.

Feige, J.N., Gerber, A., Casals-Casas, C., Yang, Q., Winkler, C., Bedu, E., Bueno, M., Gelman, L., Auwerx, J., Gonzalez, F.J., Desvergne, B., 2010. The pollutant diethylhexyl phthalate regulates hepatic energy metabolism via species-specific PPARα-dependent mechanisms. Environ. Health Perspect. 118, 234–241.

Feo, M.L., Eljarrat, E., Barceló, D., Barceló, D., 2009. Occurrence, fate and analysis of polychlorinated *n*-alkanes in the environment. TrAC, Trends Anal. Chem. 28, 778–791.

Fiedler, H., 2010. Short-chain chlorinated paraffins: production, use and international regulations. In: Boer, J. (Ed.), Chlorinated Paraffins. Springer, Berlin Heidelberg, Berlin, Heidelberg, pp. 1–40.

Gao, W., Cao, D., Wang, Y., Wu, J., Wang, Y., Wang, Y., et al., 2018. External exposure to short- and medium-chain chlorinated paraffins for the general population in Beijing, China. Environ. Sci. Technol. 52, 32–39.
Gatenby, R.A., Gillies, R.J., 2004. Why do cancers have high aerobic glycolysis? Nat. Rev. Cancer 4, 891–899.
Geng, N., Ren, X., Gong, Y., Zhang, H., Wang, F., Xing, L., et al., 2019. Integration of metabolomics and transcriptomics reveals short-chain chlorinated paraffin-induced hepatotoxicity in male Sprague-Dawley rat. Environ. Int. 133, 105231.
Gong, Y., Zhang, H., Geng, N., Xing, L., Fan, J., Luo, Y., Song, X., Ren, X., Wang, F., Chen, J., 2018. Short-chain chlorinated paraffins (SCCPs) induced thyroid disruption by enhancement of hepatic thyroid hormone influx and degradation in male Sprague Dawley rats. Sci. Total Environ. 625, 657–666.
Gong, Y., Zhang, H., Geng, N., Ren, X., Giesy, J.P., Luo, Y., et al., 2019. Short-chain chlorinated paraffins (SCCPs) disrupt hepatic fatty acid metabolism in liver of male rat via interacting with peroxisome proliferator-activated receptor α (PPARα). Ecotoxicol. Environ. Saf. 181, 164–171.
Gustafson, L.A., Kuipers, F., Wiegman, C., Sauerwein, H.P., Romijn, J.A., Meijer, A.J., 2002. Clofibrate improves glucose tolerance in fat-fed rats but decreases hepatic glucose consumption capacity. J. Hepatol. 37, 425–431.
Hong, F., Pan, S., Guo, Y., Xu, P., Zhai, Y., 2019. PPARs as nuclear receptors for nutrient and energy metabolism. Molecules 24, 2545.
Kersten, S., 2014. Integrated physiology and systems biology of PPARα. Mol. Metab. 3, 354–371.
Kersten, S., Stienstra, R., 2017. The role and regulation of the peroxisome proliferator activated receptor alpha in human liver. Biochimie 136, 75–84.
Kersten, S., Desvergne, B., Wahli, W., 2000. Roles of PPARs in health and disease. Nature 405, 421.
Klaunig, J.E., Babich, M.A., Baetcke, K.P., Cook, J.C., Corton, J.C., David, R.M., et al., 2003. PPARα agonist-induced rodent tumors: modes of action and human relevance. Crit. Rev. Toxicol. 33, 655–780.
Lau, C., Abbott, B.D., Corton, J.C., Cunningham, M.L., 2010. PPARs and xenobiotic-induced adverse effects: relevance to human health. PPAR Res. 2010, 954639.
Li, Q., Li, J., Wang, Y., Xu, Y., Pan, X., Zhang, G., Luo, C., Kobara, Y., Nam, J.J., Jones, K.C., 2012. Atmospheric short-chain chlorinated paraffins in China, Japan, and South Korea. Environ. Sci. Technol. 46, 11948–11954.
Li, H., Fu, J., Zhang, A., Zhang, Q., Wang, Y., 2016. Occurrence, bioaccumulation and long-range transport of short-chain chlorinated paraffins on the Fildes peninsula at King George Island, Antarctica. Environ. Int. 94, 408–414.
Li, T., Wan, Y., Gao, S., Wang, B., Hu, J., 2017. High-throughput determination and characterization of short-, medium-, and long-chain chlorinated paraffins in human blood. Environ. Sci. Technol. 51, 3346–3354.
Li, H., Bu, D., Fu, J., Gao, Y., Cong, Z., Zhang, G., et al., 2019. Trophic dilution of short-chain chlorinated paraffins in a plant–plateau pika–eagle food chain from the Tibetan plateau. Environ. Sci. Technol. 53, 9472–9480.
Li, H., Gao, S., Yang, M., Zhang, F., Cao, L., Xie, H., Chen, X., Cai, Z., 2020. Dietary exposure and risk assessment of short-chain chlorinated paraffins in supermarket fresh products in Jinan, China. Chemosphere 244, 125393.
Liu, L., Li, Y., Coelhan, M., Chan, H.M., Ma, W., Liu, L., 2016. Relative developmental toxicity of short-chain chlorinated paraffins in Zebrafish (*Danio rerio*) embryos. Environ. Pollut. 219, 1122–1130.
Livak, K.J., Schmittgen, T.D., 2001. Analysis of relative gene expression data using real-time quantitative PCR and the $2^{-\Delta\Delta CT}$ method. Methods 25, 402–408.
Lovekamp-Swan, T., Davis, B.J., 2003. Mechanisms of phthalate ester toxicity in the female reproductive system. Environ. Health Perspect. 111, 139–145.
Lunt, S.Y., Vander Heiden, M.G., 2011. Aerobic glycolysis: meeting the metabolic requirements of cell proliferation. Annu. Rev.Cell Dev. Biol. 27, 441–464.
Ma, X., Zhang, H., Wang, Z., Yao, Z., Chen, J., Chen, J., 2014. Bioaccumulation and trophic transfer of short chain chlorinated paraffins in a marine food web from Liaodong Bay, North China. Environ. Sci. Technol. 48, 5964–5971.
Makowski, L., Noland, R.C., Koves, T.R., Xing, W., Ilkayeva, O.R., Muehlbauer, M.J., et al., 2009. Metabolic profiling of PPARα$^{-/-}$ mice reveals defects in carnitine and amino acid homeostasis that are partially reversed by oral carnitine supplementation. The FASEB J. 23, 586–604.
Mandard, S., Müller, M., Kersten, S., 2004. Peroxisome proliferator-activated receptor α target genes. Cell. Mol. Life Sci. 61, 393–416.
Mukherjee, R., Jow, L., Noonan, D., McDonnell, D.P., 1994. Human and rat peroxisome proliferator activated receptors (PPARs) demonstrate similar tissue distribution but different responsiveness to PPAR activators. J. Steroid Biochem. Mol. Biol. 51, 157–166.
Nguyen, P., Leray, V., Diez, M., Serisier, S., Bloc'h, J.L., Siliart, B., et al., 2008. Liver lipid metabolism. J. Anim. Physiol. Anim. Nutr. 92, 272–283.
Pan, D.A., Mater, M.K., Thelen, A.P., Peters, J.M., Gonzalez, F.J., Jump, D.B., 2000. Evidence against the peroxisome proliferator-activated receptor α (PPARα) as the mediator for polyunsaturated fatty acid suppression of hepatic L-pyruvate kinase gene transcription. J. Lipid Res. 41, 742–751.
Peeters, A., Baes, M., 2010. Role of PPARα in hepatic carbohydrate metabolism. PPAR Res. 2010, 572405.
Poulsen, L.l.C., Siersbæk, M., Mandrup, S., 2012. PPARs: fatty acid sensors controlling metabolism. Semin. Cell Dev. Biol. 23, 631–639.
Qiao, L., Gao, L., Zheng, M., Xia, D., Li, J., Zhang, L., et al., 2018. Mass fractions, congener group patterns, and placental transfer of short- and medium-chain chlorinated paraffins in paired maternal and cord serum. Environ. Sci. Technol. 52, 10097–10103.
Rakhshandehroo, M., Sanderson, L.M., Matilainen, M., Stienstra, R., Carlberg, C., de Groot, P.J., et al., 2007. Comprehensive analysis of PPAR-dependent regulation of hepatic lipid metabolism by expression profiling. PPAR Res. 2007, 026839.
Rakhshandehroo, M., Knoch, B., Müller, M., Kersten, S., 2010. Peroxisome proliferator-activated receptor alpha target genes. PPAR Res. 2010, 20.
Ren, X., Zhang, H., Geng, N., Xing, L., Zhao, Y., Wang, F., Chen, J., 2018. Developmental and metabolic responses of zebrafish (*Danio rerio*) embryos and larvae to short-chain chlorinated paraffins (SCCPs) exposure. Sci. Total Environ. 622–623, 214–221.
Riedl, J., Schreiber, R., Otto, M., Heilmeier, H., Altenburger, R., Schmitt-Jansen, M., 2015. Metabolic effect level index links multivariate metabolic fingerprints to ecotoxicological effect assessment. Environ. Sci. Technol. 49, 8096–8104.
Serrone, D.M., Birtley, R.D.N., Weigand, W., Millischer, R., 1987. Toxicology of chlorinated paraffins. Food Chem. Toxicol. 25, 553–562.
Sprengel, J., Wieselmann, S., Kröpfl, A., Vetter, W., 2019. High amounts of chlorinated paraffins in oil-based vitamin E dietary supplements on the German market. Environ. Int. 128, 438–445.
Tomy, G.T., Billeck, B., Stern, G.A., 2000. Synthesis, isolation and purification of C_{10}–C_{13} polychloro-*n*-alkanes for use as standards in environmental analysis. Chemosphere 40, 679–683.
United Nations Environment Program (UNEP), 2017. The new POPs under the Stockholm Convention. http://www.pops.int/TheConvention/ThePOPs/TheNewPOPs/tabid/2511. (Accessed 31 July 2018).
van Vlies, N., Tian, L., Overmars, H., Bootsma, A.H., Kulik, W., Wanders, R.J.A., et al., 2005. Characterization of carnitine and fatty acid metabolism in the long-chain acyl-CoA dehydrogenase-deficient mouse. Biochem. J. 387, 185–193.
Wakil, S.J., Abu-Elheiga, L.A., 2009. Fatty acid metabolism: target for metabolic syndrome. J. Lipid Res. 50, S138–S143.
Wang, F., Zhang, H., Geng, N., Zhang, B., Ren, X., Chen, J., 2016. New insights into the cytotoxic mechanism of hexabromocyclododecane from a metabolomic approach. Environ. Sci. Technol. 50, 3145–3153.
Wang, F., Zhang, H., Geng, N., Ren, X., Zhang, B., Gong, Y., Chen, J., 2018. A metabolomics strategy to assess the combined toxicity of polycyclic aromatic hydrocarbons (PAHs) and short-chain chlorinated paraffins (SCCPs). Environ. Pollut. 234, 572–580.
Wu, C.C., Baiga, T.J., Downes, M., La Clair, J.J., Atkins, A.R., Richard, S.B., et al., 2017. Structural basis for specific ligation of the peroxisome proliferator-activated receptor δ. Proc. Natl. Acad. Sci. U. S. A. 114, E2563.
Xia, P., Zhang, X., Xie, Y., Guan, M., Villeneuve, D.L., Yu, H., 2016. Functional toxicogenomic assessment of triclosan in human HepG2 cells using genome-wide CRISPR-Cas9 screening. Environ. Sci. Technol. 50, 10682–10692.
Xia, D., Gao, L., Zheng, M., Li, J., Zhang, L., Wu, Y., Tian, Q., Huang, H., Qiao, L., 2017. Human exposure to short- and medium-chain chlorinated paraffins via mothers' milk in Chinese urban population. Environ. Sci. Technol. 51, 608–615.
Xu, J., Christian, B., Jump, D.B., 2006. Regulation of rat hepatic L-pyruvate kinase promoter composition and activity by glucose, *n*-3 polyunsaturated fatty acids, and peroxisome proliferator-activated receptor-αagonist. J. Biol. Chem. 281, 18351–18362.
Xu, J., Gao, Y., Zhang, H., Zhan, F., Chen, J., 2016. Dispersion of short- and medium-chain chlorinated paraffins (CPs) from a CP production plant to the surrounding surface soils and coniferous leaves. Environ. Sci. Technol. 50, 12759–12766.
Yu, S.J., Chao, J.B., Sun, J., Yin, Y.G., Liu, J.F., Jiang, G.B., 2013. Quantification of the uptake of silver nanoparticles and ions to HepG2 cells. Environ. Sci. Technol. 47, 3268–3274.
Zandbergen, F., Plutzky, J., 2007. PPARα in atherosclerosis and inflammation. Biochim. Biophys. Acta 1771, 972–982.
Zeng, L., Lam, J.C.W., Chen, H., Du, B., Leung, K.M.Y., Lam, P.K.S., 2017. Tracking dietary sources of short- and medium-chain chlorinated paraffins in marine mammals through a subtropical marine food web. Environ. Sci. Technol. 51, 9543–9552.
Zhang, Q., Wang, J., Zhu, J., Liu, J., Zhang, J., Zhao, M., 2016. Assessment of the endocrine-disrupting effects of short-chain chlorinated paraffins in *in vitro* models. Environ. Int. 94, 43–50.
Zheng, F., Zhao, X., Zeng, Z., Wang, L., Lv, W., Wang, Q., et al., 2020a. Development of a plasma pseudotargeted metabolomics method based on ultra-high-performance liquid chromatography-mass spectrometry. Nat. Protoc. 15, 2519–2537.
Zheng, X., Sun, Q., Wang, S., Li, X., Liu, P., Yan, Z., et al., 2020b. Advances in studies on toxic effects of short-chain chlorinated paraffins (SCCPs) and characterization of environmental pollution in China. Arch. Environ. Contam. Toxicol. 78, 501–512.

Supplementary material for

Exposure to short-chain chlorinated paraffins inhibited PPARα-mediated fatty acid oxidation and stimulated aerobic glycolysis *in vitro* in human cells

Yufeng Gong[1,2], Ningbo Geng[1], Haijun Zhang[1,*], Yun Luo[1,3], John P. Giesy[2,4], Shuai Sun[1,3], Ping Wu[1], Zhengkun Yu[1], Jiping Chen[1]

[1]CAS Key Laboratory of Separation Sciences for Analytical Chemistry, Dalian Institute of Chemical Physics, Chinese Academy of Sciences, Dalian, Liaoning, China

[2]Toxicology Centre, University of Saskatchewan, Saskatoon, SK, Canada

[3]University of Chinese Academy of Sciences, Beijing, China

[4]Department of Veterinary Biomedical Sciences, University of Saskatchewan, Saskatoon, SK, Canada

*Corresponding author

CAS Key Laboratory of Separation Sciences for Analytical Chemistry, Dalian Institute of Chemical Physics, Chinese Academy of Sciences, 457 Zhongshan Road, Dalian, China.

E-mail address: hjzhang@dicp.ac.cn (H. Zhang); *Telephone:* (+86) 411-8437-9972.

Number of pages: 14

Number of figures: 5

Number of tables: 1

Contents:

1. Primer sequences qPCR

Table S1. Primer sequences used in this study

Gene symbol	Description	Accession number	Primer sequence (5'-3')[1]
CPT1A	Carnitine palmitoyltransferase 1A	NM_001876	F: CAGCATATGTATCGCCTCGC R: CTGGACACGTACTCTGGGTT
CPT2	Carnitine palmitoyltransferase 2	NM_000098	F: TACGAGTCCTGTAGCACTGC R: AACAAGTGTCGGTCAAAGCC
ACSL1	Acyl-CoA synthetase long chain family member 1	NM_001995	F: GCCTCTCGCCCATATGTTTG R: CATCCGGTTCAGCAGTCTTG
ACOX1	Acyl-CoA oxidase 1	NM_004035	F: GTGACATCGGCCCCAAATTT R: AACACCATGGTCCCGTAAGT
ACADM	Acyl-CoA dehydrogenase medium chain	NM_000016	F: TCCCAGTGGCTGCAGAATAT R: AGCAGTCTGAACCCCTGTAC
EHHADH	Enoyl-CoA hydratase and 3-hydroxyacyl CoA dehydrogenase	NM_001966	F: GCCAGAAGACAGGTAAGGGT R: GCAGCTATCCCTTCTCCCAA
ACAA1	Ecetyl-CoA acyltransferase 1	NM_001607	F: GGTGGCATCAGAAATGGGTC R: GTCACAGGCACAATCTCAGC
ECI1	Enoyl-CoA delta isomerase 1	NM_001919	F: TGGTCATCAGCCTGGAGAAG R: CCTGAACGGCCTTCCAGTA
APOA5	Apolipoprotein A5	NM_052968	F: AGATAGCTGCCTTCACTCGC R: TGTCTTCCCACAGGTCATCC

PLIN2	Perilipin 2	NM_001122	F: TGACGACTACTGTGACTGGG R: CATCATCCGACTCCCCAAGA
GOT1	Glutamic-oxaloacetic transaminase 1	NM_002079	F: GGGTAGGAGGTGTGCAATCT R: TGCATCCCAGTAGCGATAGG
ELOVL6	Fatty acid elongase 6	NM_024090	F: CCGGAAGTTTGCCATGTTCA R: GCAGAAGAGCACAAGGTAGC
GAPDH	Glyceraldehyde-3-phosphate dehydrogenase	NM_002046	F: TCAAGAAGGTGGTGAAGCAGG R: TCAAAGGTGGAGGAGTGGGT

Note: Specific primers were designed based on sequence data from the GenBank (https://www.ncbi.nlm.nih.gov/genbank/)

2. Sample preparation and instrumental analysis for metabolomics

Sample preparation

Samples were mixed with 1 mL of ultrapure water, homogenized, and then ultrasonically disrupted for 5 min in an ice-water bath. The sample were subsequently freeze-dried and extracted with a mixture of methanol/water (4: 1, v: v). Soon afterwards, the solution was vortexed for 30 min, and then centrifuged for 20 min at 13,000 × g and 4 °C. Finally, the supernatant was filtered by an organic phase filter and transferred to a vial for metabolite analysis. Prior to extraction, six kinds of internal standards (i.e., Hendecanoic acid, nonadecanoic acid, *L*-phenylalanine-D^5, (8,8,8-D^3)-$_L$-carnitine, 1,2-Diheptadecanoyl-sn-glycero-3-phosphoethanolamine, and 1-lauroyl-2-hydroxy-sn-glycero-3-phosphocholine were spiked into the sample for quality control.

UHPLC/Q-TOF MS for Untargeted Tandem MS

For untargeted tandem MS, the "auto MS/MS" function of the Q-TOF MS system with data-dependent acquisition was performed in positive ion mode and negative ion mode, respectively. For positive ion mode, 5 μL of extract containing metabolites was injected into the UHPLC/Q-TOF MS system with an ACQUITY UPLC BEH C8 column (2.1 mm × 100 mm × 1.7 μm, Waters, USA) maintained at 50 °C. Water and acetonitrile both containing 0.1% (v/v) formic acid were used as mobile phases A and B, respectively. The flow rate was 0.35 mL/min, and the gradient elution was as follows (time, %B): 0 min, 10%; 3 min, 40%; 15 min, 100%, and maintained for 5 min; 20.1 min, 10%, and re-equilibrated for 2.9 min. The mass spectrometer was operated with a capillary voltage of 4000 V, fragmentor voltage of 175 V, skimmer voltage of 65 V, nebulizer gas (N_2) pressure at 45 psi, drying gas (N_2)

flow rate of 9 L/min, and a temperature of 350 °C. Five most intense precursors were chosen within one full scan cycle (0.25 s) with a precursor ion scan range of m/z 100−1000 and a tandem mass scan range of m/z 40−1000. The collision energies were set at 10, 20, 30, and 40 eV, and all samples were analyzed to obtain abundant and complementary product ion information.

For negative ion mode, 5 μL of extract containing metabolites was injected into the UHPLC/Q-TOF MS system with an ACQUITY UPLC HSS T3 column (2.1 mm × 100 mm × 1.8 μm, Waters, USA) maintained at 50 °C. Water and methanol both containing 5 mmol/L ammonium bicarbonate were used as mobile phases A and B, respectively. The flow rate was also 0.35 mL/min, and the gradient elution was as follows (time, %B): 0 min, 2%; 3 min, 42%; 12 min, 100%, and maintained for 4 min; 16.1 min, 2%, and re-equilibrated for 3.9 min. The mass spectrometer was operated with a capillary voltage of 3500 V, fragmentor voltage of 175 V, skimmer voltage of 65 V, nebulizer gas (N_2) pressure at 45 psi, drying gas (N_2) flow rate of 9 L/min, and a temperature of 350 °C. Five most intense precursors were chosen within one full scan cycle (0.25 s) with a precursor ion scan range of m/z 100−1000 and a tandem mass scan range of m/z 40−1000. The collision energies were set at −10, −20, −30, and −40 eV, and all samples were analyzed to obtain abundant and complementary product ion information.

After data acquisition, the “Find by Auto MS/MS” function of MassHunter Qualitative Analysis software was used to automatically extract ion pair information for subsequent MRM detection. The retention time window was set to 0.15 min; the MS/MS threshold was set to 100, and the mass match tolerance was set to 0.02 Da. The single mass expansion was set to symmetric 100 ppm, and the persistent background ions, such as reference mass ions, were excluded. After execution,

detected ion pairs with information about the precursor ion, product ions, retention time, and collision energy were exported to a spreadsheet. Ion pairs were selected on the basis of the following rules: different precursor ions eluted in the neighboring time range were scrutinized to exclude the isotopic, fragmentation, adduct, and dimer ions; and the product ion that appeared with the most applied collision energy and with the highest intensity was selected as the characteristic product ion.

UHPLC/Q-Trap MRM MS for Pseudo-targeted Metabolomic Analysis

A Waters Acquity Ultra Performance liquid chromatography system (UHPLC) coupled online to an ABI Q-Trap 5500 (AB SCIEX, USA) via an electrospray ionization (ESI) interface was adopted for pseudo-targeted metabolomics analysis using the spreadsheet produced from the analysis of UHPLC/Q-TOF MS. The same chromatographic condition, including chromatographic column, mobile phases, and gradient elution procedure, was performed on both UHPLC/Q-TOF MS system and UHPLC/Q-Trap MS system.

For positive ion mode, The MS instrumental parameters were set as those for the following: source temperature, 550 °C; gas I, 40 arbitrary units; gas II, 40 arbitrary units; curtain gas, 35 arbitrary units; ion spray voltage, 5500 V.

For negative ion mode, The MS instrumental parameters were set as follows: source temperature, 550 °C; gas I, 40 arbitrary units; gas II, 40 arbitrary units; curtain gas, 35 arbitrary units; ion spray voltage, −4500 V.

3. Calculation for metabolic effect level index (MELI)

In this study, the metabolic effect level index (MELI) value was calculated for each treatment group to assess the overall alteration for metabolism after different SCCPs exposure (Riedl et al., 2015). The metabolic change (MC_i) of each metabolite in a sample was calculated as follows:

$$MC_i = e^{|\ln(A_i)|} - e^{|\ln(1)|} \quad [1]$$

where A_i is the ratio of the relative abundance of a specific metabolite (i) in exposure group to the mean relative abundance of this metabolite in the control group, and ln (1) is used to subtract the metabolic level of the control group. Then, the overall metabolomics alteration of a sample was summarized as the accumulated changes of all *n* quantified metabolites according to equation [2]:

$$\text{MELI} = {\left(\sum_{i=1}^{i=n} MC_i\right)}/{n} \quad [2]$$

Reference

Riedl, J., Schreiber, R., Otto, M., Heilmeier, H., Altenburger, R., Schmitt-Jansen, M., 2015. Metabolic effect level index links multivariate metabolic fingerprints to ecotoxicological effect assessment. Environ. Sci. Technol. 49, 8096–8104.

4. MTT assays

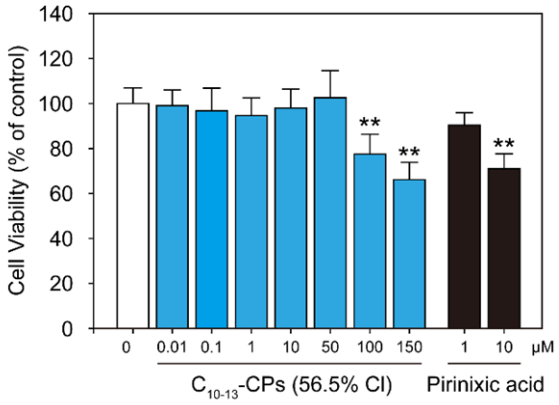

Figure S1. Viability of 293T cells exposed to $C_{10\text{-}13}$-CPs (56.5% Cl) or pirinixic acid at various concentrations for 24 hours. 0.5% DMSO served as the solvent control. Significant differences were indicated in comparison with the control. * $P < 0.05$; ** $P < 0.01$. $N = 6$.

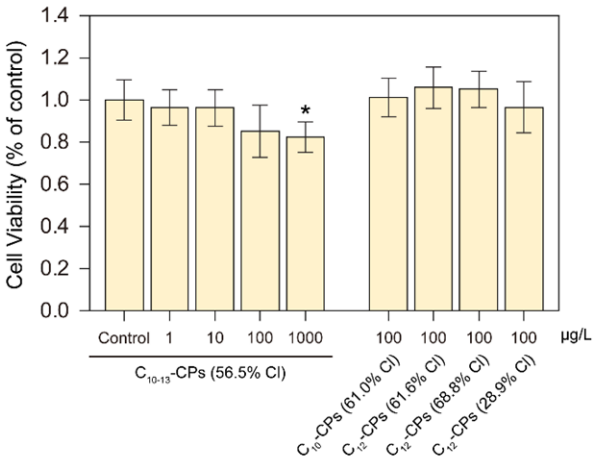

Figure S2. Viability of HepG2 cells exposed to five kinds of SCCPs mixture standards for 24 hours. SCCPs mixture standards include $C_{10\text{-}13}$-CPs (56.5% Cl), C_{10}-CPs (61.0% Cl), C_{12}-CPs (61.6% Cl), C_{12}-CPs (68.8% Cl), and C_{12}-CPs (28.9% Cl). 0.5% DMSO served as the solvent control. Significant differences were indicated in comparison with the control. * $P < 0.05$. $N = 6$.

5. Validity of luciferase assay

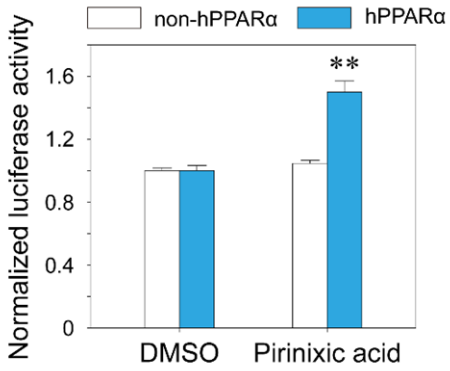

Figure S3. Transcriptional activities of human PPARα (hPPARα) by pirinixic acid at a concentration of 1 μM using *in vitro* luciferase reporter gene assay. Bars indicate the fold induction of transcriptional activities in 293T cells into which hPPARα (blue bars) or non-hPPARα (white bars) expression vector was transfected. Asterisk denotes statistical difference ($P < 0.05$; $N = 3$) from the transcriptional activities in control cells treated with 0.5% DMSO (vehicle).

6. Repeatability of pseudo-targeted metabolomics

To ensure data quality for metabolic profiling, pooled quality control (QC) samples were prepared by mixing 20 μL of metabolites extraction from all of the samples. Before analyzing the sample sequence, 4 replicates of the QC samples were run. During the analysis of the sample sequence, 7 replicates of the QC samples were inserted into the analytical sequence. For ESI^+ mode, the relative standard deviation (RSD) for the peak areas of 212 peaks detected from QC samples was calculated and the results are shown in Figure S4a. 80.57% of the 212 peaks had an RSD of less than 10%, and 99.05% of the 212 peaks had an RSD of less than 20%. Furthermore, the score plot of principal component analysis (PCA) (Figure S4c) revealed that the scores of all QC samples along the first component distributed within the confidence interval corresponding to two standard deviations (SD) ($R^2X = 0.393$), indicating that the sample analysis sequence had a satisfactory stability and repeatability.

For ESI^- mode, 68 peaks had been detected from QC samples, and the RSD for the peak areas of these 68 peaks was also calculated, and the results are shown in Figure S4b. 76.47% of the 68 peaks had an RSD of less than 10%, and 100% of the 68 peaks had an RSD of less than 20%. In addition, the score plot of PCA (Figure S4d) also indicated that the scores of all QC samples along the first component distributed within the confidence interval corresponding to two SD ($R^2X = 0.468$). The statistical results for QC samples pointed out that UHPLC/Q-Trap MS based platform had favorable repeatability for the pseudo-targeted metabolomics analysis.

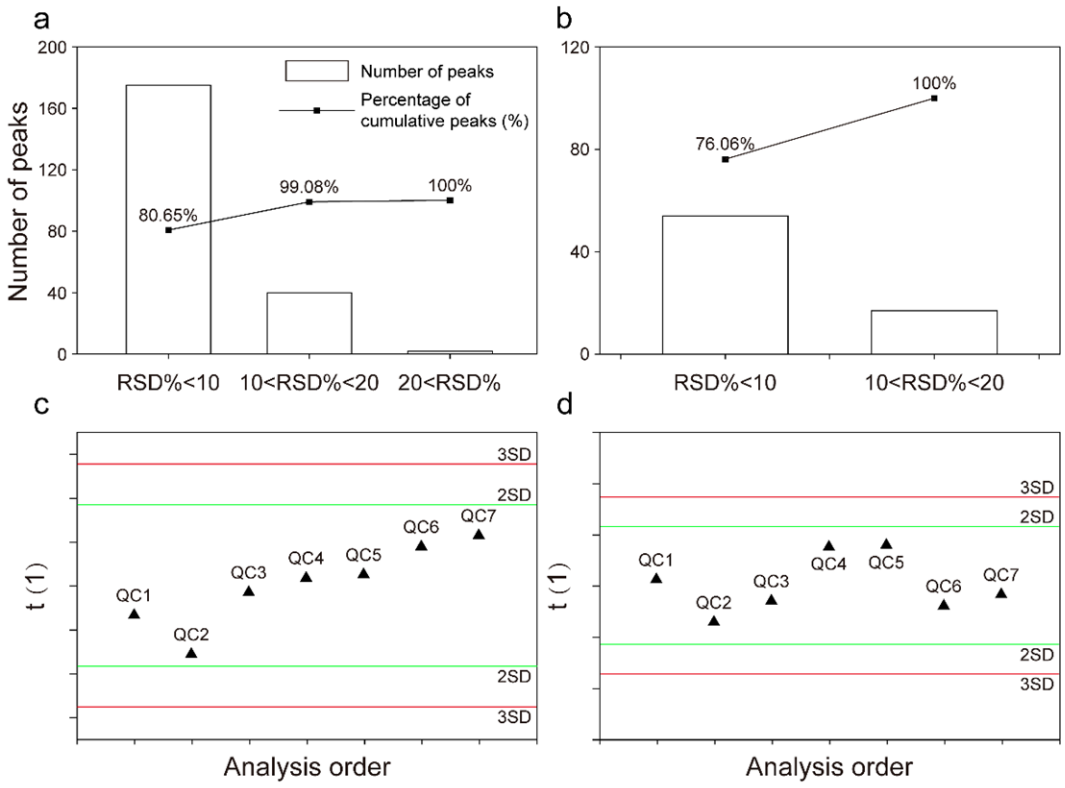

Figure S4. Distribution of % RSD and score plots of PCA for QC samples. RSD: the relative standard deviation; QC: quality control; PCA: principal component analysis. Subfigure (**a**) and (**c**) were for positive mode, while subfigure (**b**) and (**d**) were for negative mode.

7. KEGG pathway analysis of differential metabolites (DMs)

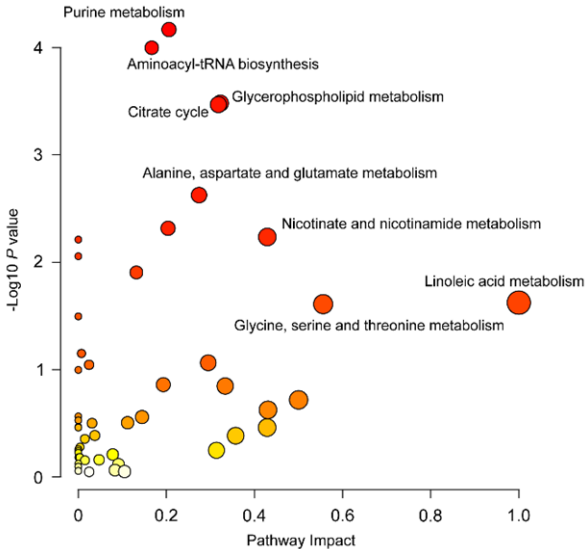

Figure S5. Most relevant metabolic pathways perturbed by exposure to SCCPs with varying chlorine contents at a concentration of 100 μg/L. Pathway analysis was performed by the MetaboAnalyst 4.0.